Available online at www.sciencedirect.com
SCIENCE DIRECT
Journal of Controlled Release 91 (2003) 157–166
journal of controlled release
www.elsevier.com/locate/jconrel

Quantification of in vivo doxorubicin transport from PLGA millirods in thermoablated rat livers

Feng Qian[a,1], Nicholas Stowe[b], Erin H. Liu[a], Gerald M. Saidel[a], Jinming Gao[a,*]

[a]*Department of Biomedical Engineering, Case Western Reserve University, Cleveland, OH 44106, USA*
[b]*Department of Surgery, Case Western Reserve University School of Medicine, Cleveland, OH 44106, USA*

Received 31 October 2002; accepted 9 January 2003

Abstract

The objective of this research was to quantify the key parameters governing the drug transport processes in radiofrequency (RF) thermoablated and non-ablated liver tissues. Experimentally, doxorubicin-containing polymer millirods were implanted in the ablated rat livers and spatial distribution of doxorubicin was measured by fluorescence imaging from 1 to 96 h after millirod implantation. At all time points, doxorubicin had significantly higher tissue penetration and retention in ablated tissues than in non-ablated tissues. A mathematical model was developed to quantitatively describe the transport processes in ablated and non-ablated rat livers. Based on the experimental data and mathematical models, the optimal estimates of apparent drug diffusivities in ablated and non-ablated tissues were 1.1×10^{-7} and 6.7×10^{-7} $cm^2\ s^{-1}$, respectively, and the apparent drug elimination rate coefficient was $9.6\times10^{-4}\ s^{-1}$ in non-ablated tissues. Results from this study contribute to the fundamental understanding of in vivo drug transport in liver tissues and provide the quantitative parameters for the rational design of polymer millirods for liver cancer treatment.
© 2003 Elsevier B.V. All rights reserved.

Keywords: Intratumoral drug delivery; Radiofrequency thermoablation; Parameter estimation; PLGA; Drug transport; Doxorubicin

1. Introduction

Polymer millirods for intratumoral drug delivery applications have been developed in our laboratory as a local chemotherapy to supplement radiofrequency (RF) ablation for the treatment of liver tumors [1–4]. The combination therapy builds on the existing expertise at our institution in developing an image-guided, minimally invasive treatment for solid tumors. Currently, image-guided RF ablation of solid tumors is under phase II clinical trials at our institution. However, liver tumors are difficult to treat by RF ablation alone due to tumor recurrence at the periphery of ablated tissue [5–7]. In the local drug therapy, a polymer implant called 'millirod' is implanted in the ablated tissue to provide a sustained release of active drug molecules to eliminate the residual cancer cells and prevent tumor recurrence.

Previously, we demonstrated that RF ablation effectively destroyed the tissue vasculature and enhanced drug penetration and retention in the

*Corresponding author. Tel.: +1-216-368-1083; fax: +1-216-368-4969.
E-mail address: jmg23@po.cwru.edu (J. Gao).
[1]Current address: Exploratory Pharmaceutics and Stability, Pharmaceutical Research Insitute, Bristol-Myers Squibb Company, New Brunswick, NJ 08903, USA.

0168-3659/03/$ – see front matter © 2003 Elsevier B.V. All rights reserved.
doi:10.1016/S0168-3659(03)00237-2

ablated liver [3]. In addition, to achieve optimal drug pharmacokinetics at the ablation boundary, we described the design of a dual-release millirod based on modeling of drug transport from millirod–tissue interface into ablated and non-ablated liver tissues [1]. The dual-release millirods have an initial burst dose to rapidly raise drug concentration at the ablation boundary to the therapeutic level, and a sustained dose to maintain the concentration for a prolonged period of time. Both the burst dose and the sustained release rate can be rationally designed if quantitative characteristics of drug transport in liver tissue are known. In the previous work, parameters of BCNU transport in brain tissues were used to demonstrate the design principle due to the lack of similar parameters in ablated liver tissues.

In this paper, we describe the quantitative study of in vivo transport properties of doxorubicin in thermoablated and non-ablated liver tissues. Doxorubicin-containing polymer millirods were implanted in thermoablated livers and the kinetics of drug distribution were characterized by fluorescence imaging over 4 days. A quantitative mathematical model was developed and implemented to provide the least-square estimates of the transport parameters (e.g., diffusivity, elimination rate coefficient) of doxorubicin in liver. Results from this study provide the fundamental understanding of drug transport in ablated livers and the necessary parameters for the rational design of polymer millirods for treatment of liver cancer.

2. Experimental methods

2.1. Materials

Poly(D,L-lactide-co-glycolide) (PLGA, lactide: glycolide=1:1, M_r 50,000 Da, inherent viscosity 0.65 dl/g) was purchased from Birmingham Polymers (Birmingham, AL, USA). Doxorubicin HCl solution (2 mg/ml in saline) was purchased from Bedford Laboratories (Bedford, OH, USA). Tris-buffered saline solution (1×) was purchased from Fisher Scientific (Pittsburgh, PA, USA). Male Sprague–Dawley rats (350–450 g) were obtained from Charles River Laboratories (Boston, MA, USA).

2.2. Millirod fabrication and in vitro characterization

The doxorubicin solution was first desalted by dialysis in distilled water. The purified doxorubicin solution was lyophilized to provide a fine powder. PLGA microspheres (mean size: 5 μm) were produced by a single emulsion procedure [4]. PLGA millirods containing 16% doxorubicin, 24% NaCl and 60% PLGA were fabricated by a compression–heat molding procedure [4]. Briefly, doxorubicin, NaCl and PLGA microspheres were weighed separately according to the final millirod composition and the three components were placed in a plastic tube and physically mixed by vortex for 10 min. The mixture was placed into a Teflon tube (1.6 mm I.D.), which was inserted inside a stainless steel mold. The mold was heated in an iso-temp oven at 90 °C (Fisher Model 282A, set point accuracy <2 °C) for 2 h to allow the annealing of the PLGA polymer. Compression pressure of 4.6 MPa was applied during the annealing process by copper weight. After cooling down to room temperature, the millirods were removed to provide the monolithic, cylindrical millirods (8 mm×1.6 mm).

To characterize the in vitro release kinetics, each millirod was placed in a glass vial containing Tris-buffered saline (2 ml) at 37 °C. The sample vial was placed in an orbital shaker (C24 model, New Brunswick Scientific) with a rotating speed of 100 rpm. At different time points, the solution was removed for doxorubicin concentration measurement followed by the addition of 2 ml fresh Tris buffer. The concentration of released doxorubicin was measured by a UV–Vis spectrophotometer (Perkin-Elmer Lambda 20 model) at its maximum adsorption wavelength (480 nm). The percentage of cumulative release was obtained by normalizing the released doxorubicin to the total amount that was loaded in the PLGA millirods (n=3).

2.3. Millirod implantation in thermoablated rat livers

Animal procedures were adhered to the NIH Guidelines and followed an approved protocol by the Institutional Animal Care and Use Committee (IACUC) at Case Western Reserve University. Male

Sprague–Dawley rats were anesthetized with an intraperitoneal injection of sodium pentobarbital (50 mg/kg). The abdomen was shaved and prepped with betadine and alcohol. A local anesthetic, Marcaine, was injected subcutaneously just prior to the skin incision. The medial lobe of the liver was exposed through a small midline incision and exteriorized for thermoablation and millirod implantation. Tissue ablation was produced using RF generated current (0.09–0.12 A) from a 19-gauge needle electrode (Radionics®, Burlington, MA, USA) at 90±2 °C for 2 min. The ablated region extended approximately 4–5 mm from the electrode surface. After the electrode was removed, a millirod was placed in the needle tract in the ablated liver. As a control study, another millirod of the same composition was implanted inside a non-ablated left lobe of the liver in the same animal.

At different time points (1, 4, 7, 24, 48 and 96 h), animals were sacrificed and polymer millirods were retrieved for the measurement of retained doxorubicin. Three animals were used for each time point. Each liver sample was removed and sectioned into two halves perpendicularly to the long axis of the millirod. One half was used for the measurement of doxorubicin concentration distribution (described below), and the other was fixed in 10% formalin solution for histological analysis. After tissue fixation, the histology samples were embedded in paraffin, sliced to a thickness of 5 μm and stained with hematoxylin and eosin (H&E). Histological photographs were taken using a Nikon Eclipse TE300 microscope.

2.4. Characterization of millirod release kinetics and tissue pharmacokinetics in vivo

Each millirod retrieved from the liver was placed in *N*,*N*-dimethylformamide (2 ml), which led to complete dissolution of the PLGA polymer and doxorubicin. The solution was diluted 10 times in Tris buffer and centrifuged to remove the precipitated PLGA polymer. The supernatant was collected and analyzed by UV–Vis spectrophotometry at 480 nm to determine the amount of doxorubicin remaining inside the millirod. The amount of released doxorubicin was calculated by the subtraction of the retained doxorubicin from the initial amount of doxorubicin in the millirod. The variation of initial drug loading density in the PLGA millirods was less than 5%. Three millirods were used to calculate the average release amount and standard deviation at each time point.

Concentration distribution of doxorubicin in rat livers was analyzed by a fluorescence imaging method as reported previously [3]. Briefly, each liver tissue sample was mounted on a cryostat chuck with O.C.T. embedding medium (Miles, Elkhart, IN, USA) and cut into 100 μm thick slices. All slices were cut perpendicular to the long axis of the millirod. The liver slices were then scanned by a fluorescence imager (FluoroImager™ SI model, Molecular Dynamics) and the fluorescence images were saved in a TIFF format with 2^{16} gray level. In the two-dimensional images, fluorescence intensity was first converted to drug concentrations based on a predetermined calibration curve [3]. Image J software was then used to determine the doxorubicin concentration as a function of distance from the millirod surface in both non-ablated and ablated tissues. The concentration–distance profile in each animal was averaged from six radial directions, with approximately 60° between each direction. The average profile at each time point was obtained from three animals in each liver environment. Optical images of the liver slices were obtained by an optical scanner (UMAX, Astra 1220s). The optical images were registered with fluorescence images to identify the ablation boundary when necessary.

3. Mathematical model and data analysis

We developed a mathematical model that describes the drug transport processes in ablated and non-ablated tissue regions. Drug enters the ablated tissue from an implanted millirod at the center of the ablated region (Fig. 1A). From the ablated tissue, it diffuses into the surrounding non-ablated region. We approximate the drug distribution in these regions assuming a cylindrical symmetry. In both regions, drug exists as both free and bound forms. Since no viable cells or blood circulation exist within the ablated region [3,8], the free drug concentration distribution changes by diffusion and drug binding, but not by perfusion or metabolism. The concen-

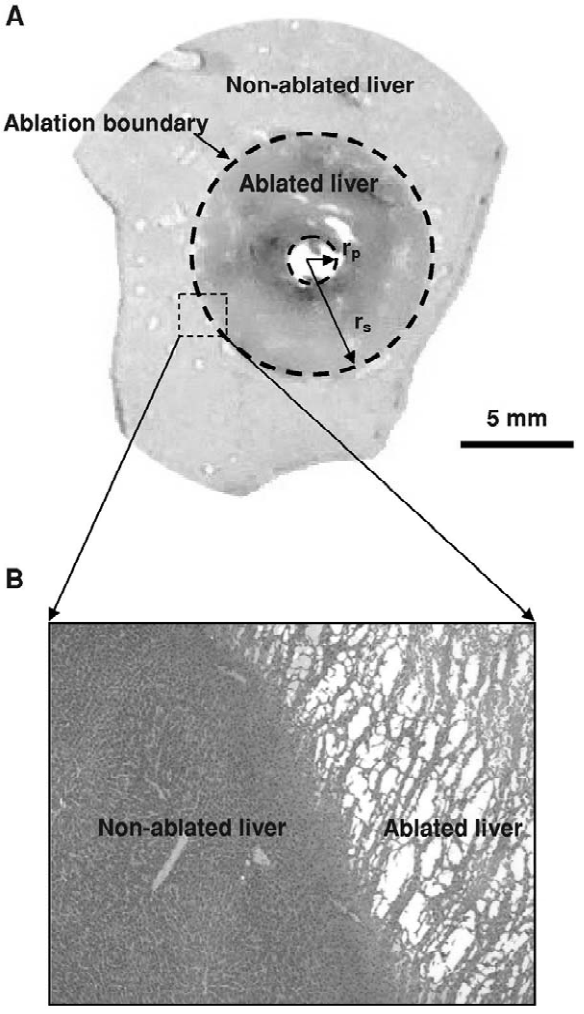

Fig. 1. (A) Optical image of a representative liver slice following RF ablation and millirod implantation. The radii of the millirod and the ablated area are denoted by r_p and r_s, respectively. (B) Histological image of the liver slice at the ablation boundary 7 h after millirod implantation. Original magnification: 40×.

trations of free and bound forms of drug in the ablated tissue, $C_{a,f}(r,t)$ and $C_{a,b}(r,t)$, respectively, change with radial position and time. The dynamics of free and bound drug concentrations (mass/tissue volume) in the ablated region ($r_p<r<r_s$) are described by:

$$\frac{\partial C_{a,f}}{\partial t} = \frac{D_a}{r}\cdot\frac{\partial[r\partial C_{a,f}/\partial r]}{\partial r} - R_a \quad (1)$$

$$\frac{\partial C_{a,b}}{\partial t} = R_a \quad (2)$$

where D_a and R_a are the diffusivity and the drug binding rate within the ablated tissue, respectively.

When the drug diffuses into the surrounding non-ablated tissue, in addition to the diffusion and binding processes, it will also be eliminated by perfusion and/or metabolism. The governing equations for the free and bound drug concentrations in the non-ablated region ($r_s<r$), $C_{n,f}(r,t)$ and $C_{n,b}(r,t)$, respectively, are:

$$\frac{\partial C_{n,f}}{\partial t} = \frac{D_a}{r}\cdot\frac{\partial[r\partial C_{n,f}/\partial r]}{\partial r} - R_n - \gamma C_{n,f} \quad (3)$$

$$\frac{\partial C_{n,b}}{\partial t} = R_n \quad (4)$$

where D_n is the diffusivity, R_n is the drug binding rate, and γ is the elimination rate coefficient for perfusion and/or metabolism in the non-ablated tissue.

By fluorescence imaging, we can only measure the total drug concentrations (mass/tissue volume) in the ablated and non-ablated tissues. Assuming both free and bound drugs distribute homogenously in each pixel volume, we obtain:

$$C_a(r,t) = C_{a,f}(r,t) + C_{a,b}(r,t) \quad (5)$$

$$C_n(r,t) = C_{n,f}(r,t) + C_{n,b}(r,t) \quad (6)$$

Therefore, we sum the free and bound equations to obtain:

$$\frac{\partial C_a}{\partial t} = \frac{D_a}{r}\cdot\frac{\partial[r\partial C_{a,f}/\partial r]}{\partial r} \quad (7)$$

$$\frac{\partial C_n}{\partial t} = \frac{D_n}{r}\cdot\frac{\partial[r\partial C_{n,f}/\partial r]}{\partial r} - \gamma C_{n,f} \quad (8)$$

To relate the free and total drug concentrations uniquely, we made an assumption similar to Fung et al. [9], that the exchange between free and bound drugs is rapid and close to equilibrium:

$$C_{a,b} = K_a C_{a,f}, \quad C_{n,b} = K_n C_{n,f} \quad (9)$$

where K_a and K_n are the drug binding constants to ablated and non-ablated tissues, respectively.

Combining Eq. (9) with Eqs. (5) and (6):

$$C_{a,f} = \frac{C_a}{1+K_a}, \quad C_{n,f} = \frac{C_n}{1+K_n} \quad (10)$$

Substitution of Eq. (10) into Eqs. (7) and (8) yields:

$$\frac{\partial C_a}{\partial t} = \frac{D_a^*}{r} \cdot \frac{\partial [r \partial C_a / \partial r]}{\partial r} \tag{11}$$

$$\frac{\partial C_n}{\partial t} = \frac{D_n^*}{r} \cdot \frac{\partial [r \partial C_n / \partial r]}{\partial r} - \gamma^* C_n \tag{12}$$

where $D_a^* = D_a/(1+K_a)$ and $D_n^* = D_n/(1+K_n)$ are the apparent diffusivities in ablated and non-ablated tissues, respectively, and $\gamma^* = \gamma/(1+K_n)$ is the apparent elimination rate coefficient.

To solve these equations, we must specify initial and boundary conditions. Initially, no drug exists in the tissue regions:

$$t = 0, \quad C_a = C_n = 0 \tag{13}$$

At the millirod–tissue interface where $C_p(t)$ is the measured concentration of drug:

$$r = r_p, \quad C_a = C_p(t) \tag{14}$$

At the boundary of ablated and non-ablated regions, the drug concentration and flux are continuous functions:

$$r = r_s, \quad C_a = C_n, \quad D_a^* \cdot \frac{\partial C_a}{\partial r} = D_n^* \cdot \frac{\partial C_n}{\partial r} \tag{15}$$

Sufficiently far from the millirod, the drug concentration will be negligible:

$$r = \infty, \quad C_n = 0 \tag{16}$$

To solve this dynamic boundary-value problem numerically, we discretized the spatial derivatives to obtain a set of differential–difference equations using well-developed software, DSS/2 (http://www.lehigh.edu/~wes1.wes1.html) [10]. The resulting initial-value problem is integrated using LSODES [11], which deals with stiff–sparse systems (http://www.netlib.org/liblist.html in odepack/lsodes.f).

Simulation of the drug distribution dynamics by solving the model equations requires specification of the model parameters: D_a^*, D_n^*, and γ^*. To estimate these parameters, we find the values that provide the best least-squares fit of the model output to the experimental data. For this purpose, we used an adaptive, nonlinear, least-squares optimization algorithm, NL2SOL (http://www.netlib.org/liblist.html in toms/573) [12]. First, we estimated D_n^* and γ^* with the experimental concentration distribution data from non-ablated tissues. Using these values, we estimated D_a^* with the experimental data from the corresponding ablated tissues. These parameters are presented in the next section.

4. Results and discussion

4.1. Tissue morphology following RF ablation

The ablated region in liver tissues is easily identified in both optical and histology images (Fig. 1). After ablation at 90 °C for 2 min, the ablated zone extended approximately 4 mm outwards from the center (Fig. 1A). In the ablated region, the cells underwent extensive coagulative necrosis, which is represented by the cells lacking a defined nuclear structure (Fig. 1B). In addition, the sinusoidal vasculature was clearly destroyed in the ablated region, leading to a loose and disorganized tissue structure. In comparison, the viable liver region is densely packed with hepatocytes and organized capillary network (Fig. 1B). These observations are consistent with a previous study of tissue morphology in ablated rabbit liver tissues [3].

Histology data of ablated tissues provides the structural basis to support our mathematical models in describing the drug transport processes. Within the ablated region, due to the cell necrosis and destruction of vasculature network, drug diffusion is the dominant mechanism of transport. Meanwhile, disrupted necrotic cells release cytoplasmic proteins or DNAs, which may lead to increased doxorubicin binding in the ablated region. In comparison, drug transport in viable liver tissues consists of drug diffusion in extracellular space, drug binding to extracellular matrix proteins, drug uptake and metabolism in hepatocytes, and drug loss due to blood perfusion through liver vasculature. Because of the experimental difficulties in differentiating each individual transport process in vivo, we used apparent diffusivity to describe the combined effect of drug diffusion and binding, and elimination rate coefficient for the combined effect of drug metabolism by cells and drug loss by perfusion (Eqs. (11) and (12)).

4.2. In vitro and in vivo doxorubicin release from PLGA millirods

Fig. 2A compares the cumulative release profiles of doxorubicin over 96 h from PLGA millirods in Tris buffer, non-ablated and ablated rat livers. During the first 48 h, more than 80% doxorubicin was released in all three environments. The half release times ($t_{1/2}$, time for 50% doxorubicin release) in Tris buffer, non-ablated and ablated livers were 8.0±3.0, 3.5±1.5 and 6.5±2.5 h, respectively. Fig. 2B compares the average doxorubicin release rates in the three environments during five time periods: 0–1, 1–4, 4–7, 7–24 and 24–48 h. In the first two time periods, the average doxorubicin release rate is slightly faster in non-ablated livers than that in ablated livers. In addition, the average release rates in both liver environments are slightly faster than that in Tris buffer. It should be noted that within any of the time periods, none of the differences in average release rates are significant.

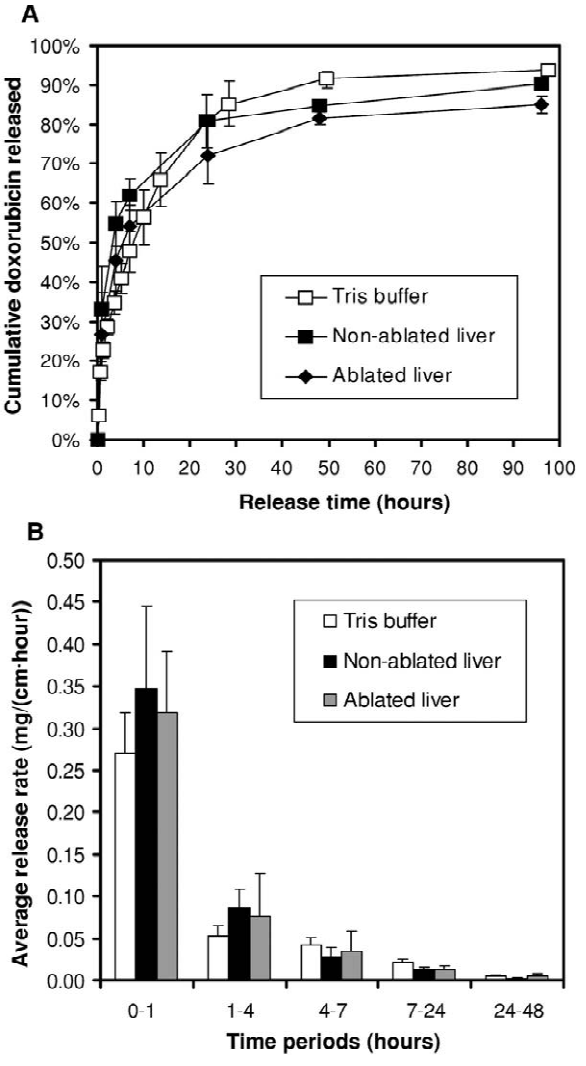

Fig. 2. (A) Cumulative release profiles of doxorubicin from PLGA millirods in Tris buffer, non-ablated livers and ablated livers. (B) Average doxorubicin release rates in the above three environments during five time periods: 0–1, 1–4, 4–7, 7–24 and 24–48 h.

Based on the $t_{1/2}$ values, the doxorubicin release in non-ablated livers (3.5±1.5 h) is slightly faster than that in ablated livers (6.5±2.5 h). In both liver environments, there are plenty of fluids surrounding the implants. In the non-ablated tissues, the fluids come from blood circulation through liver vasculature and/or bile flow inside the bile ducts. In comparison, the ablated tissues undergo acute inflammation in the wound healing process, in which exudation of fluid and plasma proteins (edema) occurs [13]. The edematization process provides fluids to the ablated region and facilitates the release of doxorubicin from the millirods. The slightly faster release kinetics of doxorubicin in non-ablated tissues over ablated tissues may be a result of blood perfusion in non-ablated tissues, which carries away the drug molecules and leads to a higher concentration gradient at the millirod–tissue interface. This hypothesis is further supported by a previous study of the release kinetics of a different molecule, iohexol (a CT contrast agent), where an approximately twofold increase of $t_{1/2}$ was observed in ablated (20.6±5.9 h) than non-ablated liver tissues (12.1±5.4 h) [8]. In the current study, we also observed relatively slower release of doxorubicin in Tris buffer (8.0±3.0 h) compared to those in liver tissues. We hypothesize that plasma proteins in the in vivo studies serve as detergent molecules to solubilize doxorubicin (a hydrophobic drug), which subsequently facilitates the drug release from the polymer millirods. Current work is in progress to examine the effect of added plasma proteins in Tris buffer on in vitro release kinetics of doxorubicin from PLGA millirods.

4.3. Kinetics of doxorubicin distribution in liver tissues

Fig. 3 shows a series of representative fluorescent images of liver slices from ablated and non-ablated liver tissues at different implantation times. By gross inspection, doxorubicin distribution in non-ablated liver tissues was limited to the implantation sites; almost no detectable amount of doxorubicin was found 1 mm away from the millirod–tissue interface at any time points. In comparison, the doxorubicin distribution in ablated tissues was much larger than that in non-ablated tissue at all times. After 7 h, the radius of the drug distribution region reached 4–5 mm, which appeared to be larger than the radius of the ablated tissue (~4 mm).

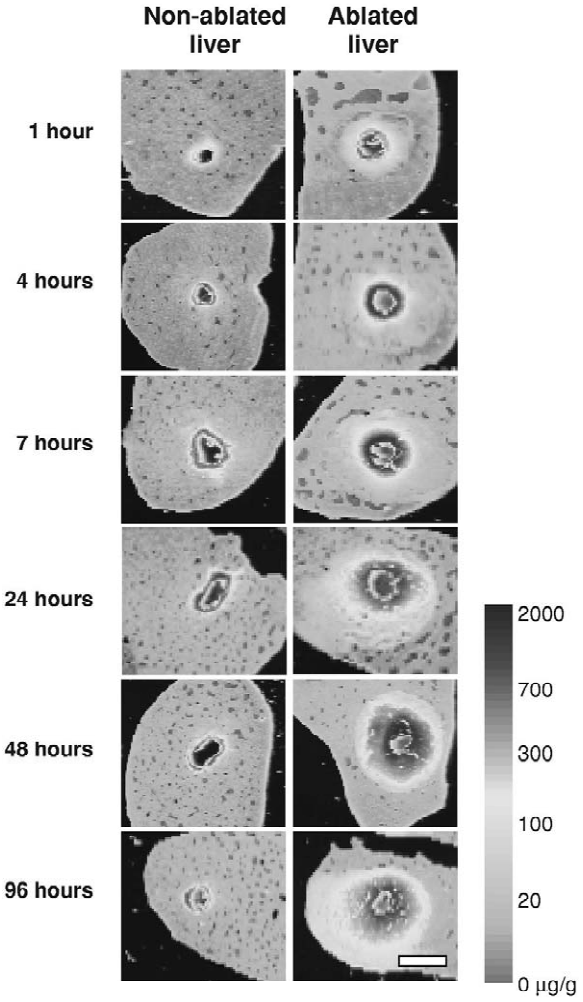

Fig. 3. Fluorescence images of doxorubicin concentration distribution in non-ablated and ablated rat livers from 1 to 96 h. The color bar represents the range of doxorubicin concentration in liver tissues. The scale bar (5 mm) in the bottom right image applies to all the other images.

Fig. 4 shows the quantitative concentration distributions of doxorubicin in non-ablated and ablated liver tissues at different implantation times. At all times, doxorubicin had significantly more penetration and retention in the ablated tissue than the non-ablated tissue. In the ablated tissue, the pattern of distribution increased steadily from 1 to 24 h. From 24 to 96 h, the drug distribution profiles changed a little, with the doxorubicin concentrations at the millirod/tissue interface decreasing slightly from 1.7 mg/g at 24 h to 1.4 mg/g at 96 h (Fig. 4). Because more than 70% of doxorubicin was released from the PLGA millirods after 24 h (Fig. 2A) and the release rates in 24–48 and 48–96 h periods were very low (Fig. 2B), we attribute the high doxorubicin retention in ablated tissues at 48 and 96 h mostly to the drug binding to macromolecules (e.g., proteins, DNA), which is consistent with literature reports [14–16].

To examine the therapeutic relevance of drug penetration, we defined the therapeutic distance (TD) as the distance at which doxorubicin concentration reaches 6.4 μg/g, the cytotoxic concentration of doxorubicin for VX-2 tumor cells [17]. The TD value changed with time in non-ablated and ablated liver tissues, and the results are shown in Fig. 5. In non-ablated tissues, the TD value reached a maximum of 1.1±0.1 mm 24 h after millirod implantation, and then decreased to 0.3±0.1 mm at 96 h. In ablated tissues, the TD value reached 4.1±0.2 mm at 7 h and remained at approximately 4 mm until 96 h. At all time points, the TD values in ablated tissues are 4–10-times larger than those in non-ablated tissues. These results clearly demonstrate the advantage of RF ablation in facilitating drug penetration to achieve a significantly larger therapeutic margin by local drug therapy.

4.4. Parameter estimation and simulations

Doxorubicin concentration at the millirod/tissue interface was analyzed and used as one of the

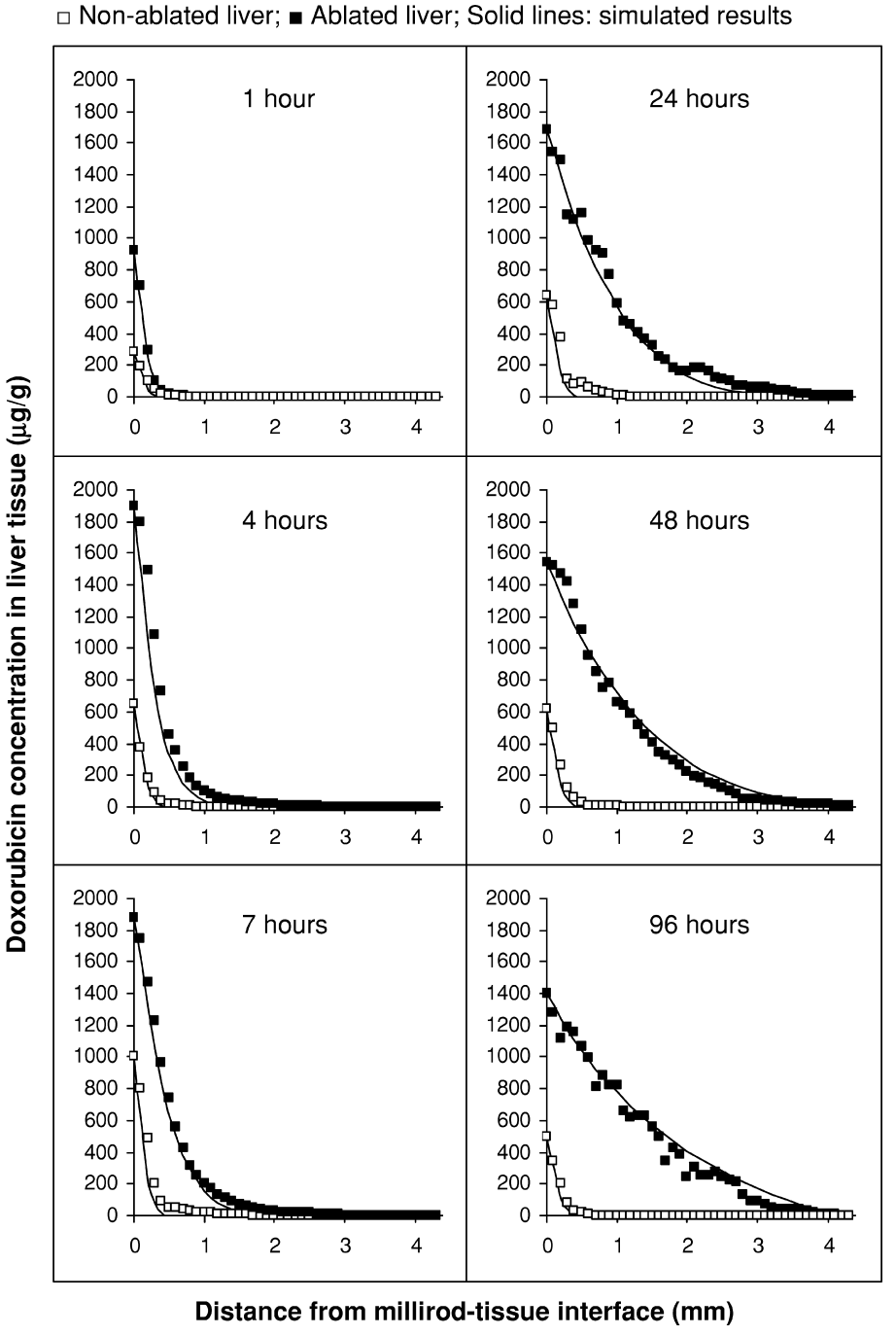

Fig. 4. Quantitative concentration distribution profiles of doxorubicin in non-ablated and ablated rat livers. Dots represent the experimental data (□: in non-ablated tissue, ■: in ablated tissue). Each experimental profile represents an average result of eight directions from millirod–tissue interface for three animals. For clarity of presentation, the error bars were omitted for each data point. Solid lines represent model simulation results. Parameters used: $D_a^* = 1.1\times10^{-7}$ cm^2 s^{-1}, $D_n^* = 6.7\times10^{-7}$ cm^2 s^{-1}, $\gamma^* = 9.6\times10^{-4}$ s^{-1}. For easy comparison, the scales of both distance and concentration axis are kept identical for all six time points.

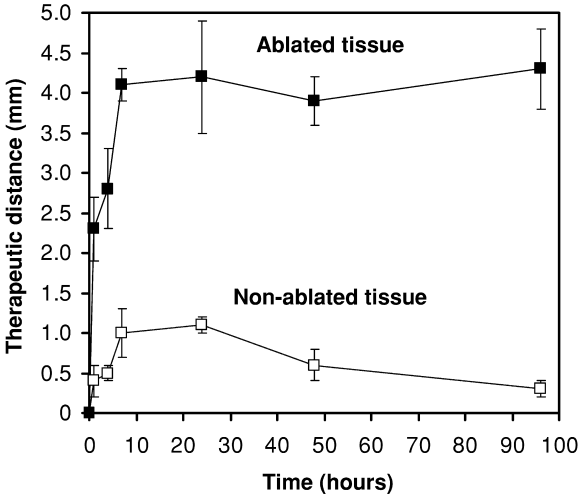

Fig. 5. Therapeutic distance of doxorubicin at different implantation times in non-ablated (□) and ablated (■) liver tissues ($n=3$).

boundary conditions (Eq. (14)) in the estimation of model parameters. In both non-ablated and ablated tissues, drug concentrations at the interface increased rapidly in the first several hours and thereafter decreased slowly (Fig. 6). The interface concentration in the ablated tissues was approximately 2–3-times higher than that in the non-ablated tissues.

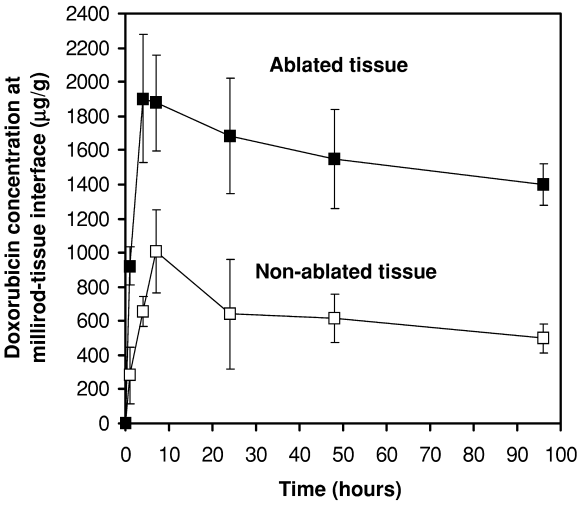

Fig. 6. Concentration–time curve of doxorubicin at millirod–tissue interface in non-ablated (□) and ablated (■) liver tissues ($n=3$).

Based on the experimental data in Fig. 4 and previously described mathematical models, we obtained the quantitative estimation of the transport parameters in non-ablated and ablated liver tissues. The optimal estimate of the apparent doxorubicin diffusivity in ablated livers (D_a^*) was ranged from 0.8×10^{-7} to 1.3×10^{-7} cm^2 s^{-1} in three experimental groups, and that in non-ablated livers (D_n^*) from 5.8×10^{-7} to 8.2×10^{-7} cm^2 s^{-1}. The optimal estimate of the apparent drug elimination coefficient (γ^*) in non-ablated tissue was ranged from 4.2×10^{-4} to 15.6×10^{-4} s^{-1}. Using the average values of the estimated parameters ($D_a^*=1.1\times10^{-7}$ cm^2 s^{-1}, $D_n^*=6.7\times10^{-7}$ cm^2 s^{-1}, $\gamma^*=9.6\times10^{-4}$ s^{-1}), we simulated doxorubicin concentration profiles in both non-ablated and ablated liver tissues (Fig. 4, solid lines) that correspond closely to the experimental data (Fig. 4, dots).

The estimated apparent diffusivity of doxorubicin is approximately six-times smaller in ablated livers than that in non-ablated livers. This is presumably the result of a greater drug binding effect in the ablated tissue, which is shown as a larger binding constant in the definition of the apparent diffusivity. Otherwise, one would expect that the diffusion coefficient to be greater in the ablated tissue because of the reduction of structural barriers (Fig. 1B). Although the apparent drug diffusivity is less in the ablated than non-ablated tissues, drug penetration is significantly larger in ablated tissues. In the ablated tissues, the absence of blood perfusion reduces drug loss and results in the increased penetration distance of doxorubicin. Although the in vivo transport processes are complicated, we found that the current mathematical models (e.g., Eqs. (11) and (12)) combined with key transport parameters (D_a^*, D_n^*, γ^*) permitted a simple and accurate description of the dynamics of drug distribution in liver tissues (Fig. 4).

5. Conclusion

This paper investigated the in vivo release kinetics of doxorubicin from polymer millirods and the drug transport properties in non-ablated and ablated liver tissues. Fluorescence imaging studies demonstrated

larger tissue penetration and retention of doxorubicin in ablated livers than non-ablated livers. Based on the experimental concentration distribution profiles and mathematical models, we determined the quantitative transport parameters of doxorubicin in the two tissue environments. The apparent drug diffusivities in ablated and non-ablated livers are 1.1×10^{-7} and 6.7×10^{-7} cm^2 s^{-1}, respectively, and the apparent drug elimination rate coefficient is 9.6×10^{-4} s^{-1} in non-ablated livers. These parameters provide the essential data for the quantitative design of dosage regimens of dual-release millirods [1] in the treatment of liver cancers.

Acknowledgements

This work is supported by a research grant from the National Institute of Health (R01-CA-90696).

References

[1] F. Qian, G.M. Saidel, D.M. Sutton, A. Exner, J. Gao, Combined modeling and experimental approach for the development of dual-release polymer millirods, J. Control. Release 83 (2002) 427–435.
[2] F. Qian, N. Nasongkla, J. Gao, Membrane-encased polymer millirods for sustained release of 5-fluorouracil, J. Biomed. Mater. Res. 61 (2002) 203–211.
[3] J. Gao, F. Qian, A. Szymanski-Exner, N. Stowe, J. Haaga, In vivo drug distribution dynamics in thermoablated and normal rabbit livers from biodegradable polymers, J. Biomed. Mater. Res. 62 (2002) 308–314.
[4] F. Qian, A. Szymanski, J. Gao, Fabrication and characterization of controlled release poly(D,L-lactide-co-glycolide) millirods, J. Biomed. Mater. Res. 55 (2001) 512–522.
[5] G.D. Dodd III, M.C. Soulen, R.A. Kane, T. Livraghi, W.R. Lees, Y. Yamashita, A.R. Gillams, O.I. Karahan, H. Rhim, Minimally invasive treatment of malignant hepatic tumors: at the threshold of a major breakthrough, Radiographics 20 (2000) 9–27.
[6] R. Lencioni, O. Goletti, N. Armillotta, A. Paolicchi, M. Moretti, D. Cioni, F. Donati, A. Cicorelli, S. Ricci, M. Carrai et al., Radio-frequency thermal ablation of liver metastases with a cooled-tip electrode needle: results of a pilot clinical trial, Eur. Radiol. 8 (1998) 1205–1211.
[7] L. Buscarini, S. Rossi, Technology for radiofrequency thermal ablation of liver tumors, Semin. Laparosc. Surg. 4 (1997) 96–101.
[8] A. Szymanski-Exner, N.T. Stowe, R.S. Lazebnik, K. Salem, D.L. Wilson, J.R. Haaga, J. Gao, Noninvasive monitoring of local drug release in a rabbit radiofrequency (RF) ablation model using X-ray computed tomography, J. Control. Release 83 (2002) 415–425.
[9] L.K. Fung, M. Shin, B. Tyler, H. Brem, W.M. Saltzman, Chemotherapeutic drugs released from polymers: distribution of 1,3-bis(2-chloroethyl)-1-nitrosourea in the rat brain, Pharm. Res. 13 (1996) 671–682.
[10] W.E. Schiesser, C. Silebi, Computational Transport Phenomena, Cambridge University Press, Cambridge, 1997.
[11] A.C. Hindmarsh, ODEPACK, A systemized collection of ode solvers. In: Scientific computing, R.S. Stepleman (Ed.), North Holland, Amsterdam, 1983, pp. 509–516.
[12] J.E. Dennis, D.M. Gay, R.E. Welsch, An adaptive nonlinear least-squares algorithm, ACM Trans. Math. Software 7 (1981) 348–368.
[13] J. Anderson, Mechanisms of inflammation and infection with implanted devices, Cardiovasc. Pathol. 2 (1993) 33S–41S.
[14] B. Chauffert, M. Dumas, A. Dubuet, P.D. Athis, N.O. Olsson, Differential retention of doxorubicin in the organs of two strains of rats, J. Pharm. Pharmacol. 40 (1988) 97–100.
[15] T. Terasaki, Y. Iga, Y. Sugiyama, M. Hanano, Interaction of doxorubicin with nuclei isolated from rat liver and kidney, J. Pharm. Sci. 34 (1984) 524–528.
[16] M. Rozencweig, Y. Kenis, G. Atassi, M. Staquet, M. Duarte-Karim, DNA–adriamycin complex: preliminary results in animals and man, Cancer Chemother. Rep. Part 3 6 (1975) 131–136.
[17] J.A. Ridge, C. Collin, J.R. Bading, C. Hancock, P.S. Conti, J.M. Daly, J.H. Raaf, Increased adriamycin levels in hepatic implants of rabbit Vx-2 carcinoma from regional infusion, Cancer Res. 48 (1988) 4584–4587.